Rakenteiden Mekaniikka (Journal of Structural Mechanics)
Vol. 55, No. 4, 2022, pp. 95–115
https://rakenteidenmekaniikka.journal.fi/index
https://doi.org/10.23998/rm.120470

VERTAISARVIOITU
KOLLEGIALT GRANSKAD
PEER-REVIEWED
www.tsv.fi/tunnus

The coupling of solids and shells by conjugate approximations

Mika Malinen[1] and Peter Råback

Summary In order to get detailed information about deformations of structures efficiently, it may be necessary to use finite element models which combine three-dimensional discretizations of solids with approximations of two-dimensional models for shells. Here we show how the idea of conjugate approximations can be used as a means to obtain a formulation of mixed-dimensional coupling between shells and solids. Our method is consistent with respect to the principle of virtual work and does not depend on additional computational parameters, an augmentation of a potential-energy functional by introducing new unknowns, or computations over auxiliary meshes.

Key words: mixed-dimensional coupling, shell, finite element, biorthogonal basis, tight coupling

Received: 30 June 2022. Accepted: 3 February 2023. Published online: 13 February 2023.

Introduction

It is common that finite element analysis of a structure which is a mixture of thin shell-like bodies and relatively massive solids is needed. Similarly, in order to get detailed information about deformations of thin bodies efficiently, it may be necessary to use refined models which combine local three-dimensional discretizations of solids with approximations of two-dimensional models for shells [9, 3] based on dimensional reduction. For example, such analyses may be important in order to fully account for boundary layers. These needs necessitate the development of special techniques to handle mixed-dimensional couplings so that the difference in the dimensionality of the constituent models can be handled.

Given the development of high-speed computers, a seemingly natural approach to avoid the problem of mixed-dimensional coupling would be to apply only three-dimensional discretizations. However, thinness causes several troubles in practice. Firstly, standard low-order finite elements cannot in general be used to obtain reliable solutions for shells, since these methods suffer from approximation failures resulting in numerical overstiffness (locking). In the case of very thin shells, loss of significance errors may also be a serious trouble, especially when the solid finite elements based on nodal unknowns are used in the computation. Therefore, the discretization over a solid should either be based on (hierarchic) high-order finite elements or be based on special low-order formulations

[1]Corresponding author: mika.malinen@csc.fi

that account for locking. We note that much of this work to construct locking-free finite elements for shell-like bodies is however limited to the two-dimensional (surface) representations of shells, i.e., accounts of suitable three-dimensional formulations are far less numerous. Secondly, generating a conforming three-dimensional finite element mesh may require an excessive mesh refinement in order to fit a thin three-dimensional body. If the requirement of having a conforming discretization was relaxed, the need for handling additional constraint equations would again arise, albeit in a different form. On the other hand, although there is a modern trend that new shell finite elements are increasingly three-dimensional by using richer kinematic assumptions over the thickness, they are not usually considered as alternatives to discretize a massive body, i.e., the assumption of thinness is still vital in their derivation.

We note that different approaches to handle mixed-dimensional couplings have been proposed in literature. They include the use of special transition finite elements [12], handling multipoint constraint equations [4], applying formulations based on Nitche's method [13], and iterative procedures that couple a global two-dimensional model with a local three-dimensional model via using overlapping decompositions [5]. We note that the use of transition finite elements involves the burden of constructing new finite element types and also complicates the preprocessing step of analysis, as special connectivity of degrees of freedom has to be applied over a local mesh consisting of them.

On the other hand, in the case of hyperelasticity that enables us to describe our structural analysis problem in terms of an energy functional, a general strategy to handle multipoint constraint equations is obtained by the method of Lagrange multipliers, at the cost of introducing additional unknowns. Here different approaches may be used to derive the actual constraint equations. They can be generated by purely kinematic considerations, but energy arguments (such as work equilibration) may also be applied in the derivation [11]. It is notable that the augmentation of a potential-energy functional in terms of the Lagrange multipliers gives rise to a discrete saddle point problem whose efficient solution with iterative methods may become less straightforward [1]. The formulations based on Nitche's method have the benefit that they avoid the introduction of additional unknowns, but an additional computational stabilization (penalty) parameter has to be introduced. As an alternate to using the Lagrange multipliers, the penalty methods have also been applied to handle multipoint constraint equations, but the questions of consistency and computational accuracy may then arise. For a sampling of earlier work on the subject of this paper, see, for example, papers cited in [13].

It should be noted when Lagrange multipliers are introduced for enabling the coupling of structural models, there are some subtleties in their interpretation. If the solution of shell equations is naturally extended to the three-dimensional body associated with the mid-surface of the shell, the interaction between the shell model and the solid model can be considered to occur on a two-dimensional surface Γ, which contains a spatial curve giving the intersection of the mid-surface and the solid. The concept of surface coupling is thus introduced in a natural way and using a weak formulation over Γ to obtain the coupling constraints leads to considering a Lagrange multiplier as a member in a suitable function space on Γ. The choice of this function space may be expected to be an essential ingredient to obtain stability, which may not in general be immediate as saddle point methodology is employed. However, in engineering literature multipoint constraints are typically treated by using Lagrange multipliers without referring to function spaces. That is, the Lagrange multipliers are introduced after the generation of multipoint constraints when the linear algebraic equations of the augmented problem are assembled; cf., the treatment in [4].

The Lagrange multipliers are then interpreted just as discrete (generalized) forces applied through points on the coupling interface Γ.

The apparent differences in the descriptions of Lagrange multipliers discussed above are interesting and are also our source of inspiration here. We shall investigate such aspects by considering a regular reconstruction of force fields from pointwise reactions (generalized forces), which are often routinely computed in finite element analyses of specific problems and which are now closely related to the possible interpretations of Lagrange multipliers. We note that such reconstruction is subject to a priori choice of regularity in a manner reminiscent of choosing a suitable function space for a Lagrange multiplier. Here our reconstruction is a global field and is as smooth as the primary finite element approximation (that is, H^1-regular), so we avoid an irregular reconstruction in the sense of distributions. These considerations finally bring us to new ideas to formulate coupled structural models without introducing either adjustable computational parameters or Lagrange multipliers as additional unknowns. In addition, this process is possible without considering the coupling interface Γ as a two-dimensional surface and performing auxiliary computations over it like those used in [11]. A relevant theory which we apply in our development was put forward in a paper [2] on conjugate approximations published already in the early 1970's.

Our plan is first to outline the development of a specialized shell model from a three-dimensional energy principle and to introduce very basic concepts of conjugate approximations (which suffice for our purposes) in the next two sections. In the next few sections after these preliminaries, we then show how the concepts introduced can be applied to construct a model for shell-solid coupling. We shall start with a somewhat generalized variational formulation of the field equations over each domain in order to include (generalized) forces, which are considered to be either forces exerted on the solid by the shell body or coupling reactions occurring when the shell body is constrained to obey the deformation of the solid (therefore, the idea of using a domain decomposition of Dirichlet-Neumann type is inherent in our derivation, but we emphasize that our solution strategy handles all equations simultaneously). We then use conjugate approximations to represent these forces between the constituent parts, so that we can explicitly construct the linear functionals of the variational formulation that account for the coupling forces. We note that in order to introduce the key ideas in a simple way we shall start with the case of the coupling of two three-dimensional models, which is usually treated routinely without any reference to conjugate approximations.

This theoretical development culminates in a proof of the satisfaction of work equilibration of (generalized) coupling forces. This result is of both practical and theoretical importance by ensuring that the total potential-energy functional of the coupled structure has a natural decomposition into two expressions over a solid and a shell domain, so that no perturbation of energy is associated with the coupling forces. The formulation of this property is notable in its conciseness, as we do not need for example definitions over auxiliary meshes. The rest of the paper covers some implementation aspects, shows the utility by computational examples and also includes some concluding remarks. In regard to the implementation, we also discuss the possibilities of simplifying approximations so that some global computations needed in the precise computation of conjugate basis functions can be avoided. Our implementation, used in the computational examples of this paper, is available within open source FEM software Elmer [10].

Models for structures

The constraint equations needed in mixed-dimensional coupling between shells and solids depend crucially on the choice of equations used to approximate deformations of shells. Here we shall consider hyperelastic bodies, so that energy arguments can be applied in order to simplify the shell model under kinematic assumptions. To simplify our presentation, the formulation of linearized and static equations is only treated.

Our assumption about hyperelastic bodies enable us to seek equilibrium states by seeking those states that minimize the potential-energy functional for the structure under suitable subsidiary conditions. Here the kinematic assumptions on the displacement field $\boldsymbol{u}$ are assumed to be of sufficient richness, so that the strain-energy function $W(\cdot, \boldsymbol{\varepsilon}(\boldsymbol{u}))$ as a function of place can be parametrized consistently by all component functions $\varepsilon_{ij}(\boldsymbol{u})(\cdot)$ of the three-dimensional strain tensor field $\boldsymbol{\varepsilon}(\boldsymbol{u})$ over the entire structure, consisting of bodies which are either thin or unsuitable for analysis with shell models. The total stored energy in the structure may thus be decomposed as

$$\mathcal{U}(\boldsymbol{u}) = \int_{\Omega} W(\cdot, \boldsymbol{\varepsilon}(\boldsymbol{u}))\mathrm{d}\Omega + \int_{\widehat{\Omega}} W(\cdot, \boldsymbol{\varepsilon}(\boldsymbol{u}))\mathrm{d}\widehat{\Omega}, \tag{1}$$

where $\widehat{\Omega} \subset \mathbb{E}^3$ represents the thin parts. We may then define the potential-energy functional by

$$\Pi(\boldsymbol{u}) = \mathcal{U}(\boldsymbol{u}) + \mathcal{F}(\boldsymbol{u}), \tag{2}$$

where $\mathcal{F}(\boldsymbol{u})$ is the potential energy of the forces applied to structure, having an analogous decomposition into two expressions over Ω and $\widehat{\Omega}$.

The shell body $\widehat{\Omega}$ is taken to consist of points within a small distance from its mid-surface $\mathcal{S} \subset \mathbb{E}^3$. We assume that any point $\mathbf{x} \in \widehat{\Omega}$ has a unique representation in normal coordinates as

$$\mathbf{x} = \mathbf{s} + y^3 \boldsymbol{d}(\mathbf{s}), \tag{3}$$

where $\boldsymbol{d} : \mathcal{S} \to \mathbb{R}^3$ is a unit vector (director) field and $y^3 \in [-d/2, d/2]$, with d being the shell thickness. If we let $\boldsymbol{\varphi} : \omega \to \mathcal{S}$, with $\omega \subset \mathbb{R}^2$, be a parametrization of the mid-surface, the full representation of $\widehat{\Omega}$ in three curvilinear coordinates is obtained by rewriting (3) as

$$\mathbf{x} = \boldsymbol{\Theta}(\mathbf{y}, y^3) \equiv \boldsymbol{\varphi}(\mathbf{y}) + y^3(\boldsymbol{d} \circ \boldsymbol{\varphi})(\mathbf{y}), \tag{4}$$

with $\mathbf{y}$ being a 2-tuple (y^1, y^2), and by letting the function $\boldsymbol{\Theta}^{-1} : \widehat{\Omega} \to \mathbb{R}^3$ assign a triple of curvilinear coordinates (y^1, y^2, y^3) to each point $\mathbf{x}$ in the shell.

In view of the representation (3), it is natural to approximate the displacement vector field of the shell

$$(\mathbf{s}, y^3) \mapsto \boldsymbol{u}(\mathbf{s}, y^3) \tag{5}$$

in a systematic manner by representing it as a power series in the thickness coordinate. Here we consider an approximation in the form

$$\boldsymbol{u}(\boldsymbol{\varphi}(\mathbf{y}), y^3) \equiv \boldsymbol{v}(\mathbf{y}) - y^3 \boldsymbol{\beta}(\mathbf{y}) - \frac{1}{2}(y^3)^2 \boldsymbol{\psi}(\mathbf{y}), \tag{6}$$

where the part $\boldsymbol{\psi}(\mathbf{y})$ can be expressed simply as

$$\boldsymbol{\psi}(\mathbf{y}) = [\boldsymbol{a}_3(\mathbf{y}) \cdot \boldsymbol{\psi}(\mathbf{y})]\boldsymbol{a}^3(\mathbf{y}), \tag{7}$$

with $\boldsymbol{a}_3(\mathbf{y}) = \boldsymbol{a}^3(\mathbf{y}) = (\boldsymbol{d} \circ \boldsymbol{\varphi})(\mathbf{y})$.

The stored energy and the potential energy of forces for the shell can be simplified in many ways by integrating over the shell thickness, by omitting terms involving higher powers of the ratio of the shell thickness to a characteristic radius of curvature, and by using an orthogonal (re-)parametrization of the mid-surface [7]. In addition, a work presented in [6] shows that the model which employs the displacement parametrization in terms of a 7-tuple of scalar fields according to (6) and (7) can be simplified in an asymptotically correct manner into a 6-parameter model. We note that in [6] a basic material described by two Lamé coefficients was assumed, but a generalization to allow a more general class of materials and also nonlinearities is possible. For the simplified expressions of the stored energy and the potential energy of forces such that the energy densities for the 6-parameter shell model are expressed over the shell mid-surface, see [6] and also [10].

When the asymptotically correct simplification into a 6-parameter shell model is employed, the primary unknowns of the shell model are related to the three-dimensional displacement $\boldsymbol{u} : \mathcal{S} \times [-d/2, d/2] \to \mathbb{R}^3$ by

$$\begin{aligned} (\boldsymbol{v} \circ \boldsymbol{\varphi}^{-1})(\mathbf{s}) &= \boldsymbol{u}(\mathbf{s}, 0), \\ (\boldsymbol{\beta} \circ \boldsymbol{\varphi}^{-1})(\mathbf{s}) &= -D\boldsymbol{u}(\mathbf{s}, 0)[\boldsymbol{d}], \end{aligned} \tag{8}$$

where the directional derivative is defined by

$$D\boldsymbol{u}(\mathbf{s}, 0)[\boldsymbol{d}] = \lim_{\alpha \to 0} \frac{\boldsymbol{u}(\mathbf{s}, \alpha) - \boldsymbol{u}(\mathbf{s}, 0)}{\alpha}. \tag{9}$$

This model is interesting from the viewpoint that, in connection with lowest-order finite elements, the relations (8) in principle enable an easy computation of the constraints of Dirichlet type, so that the edge displacement of the shell can be made to follow the displacement of the solid. That is, if we had a perfectly regular mesh, we could create the nodal constraints of Dirichlet type such that

$$\begin{aligned} (\boldsymbol{v} \circ \boldsymbol{\varphi}^{-1})(\mathbf{s}_k) &= \frac{\boldsymbol{u}_k^+ + \boldsymbol{u}_k^-}{2}, \\ (\boldsymbol{\beta} \circ \boldsymbol{\varphi}^{-1})(\mathbf{s}_k) &= -\frac{\boldsymbol{u}_k^+ - \boldsymbol{u}_k^-}{d}, \end{aligned} \tag{10}$$

where $\boldsymbol{u}_k^+$ and $\boldsymbol{u}_k^-$ denote the solid displacements at the nodes which are located on the upper and lower faces of the three-dimensional shell and met when proceeding from the node $\mathbf{s}_k$ in the direction of either positive or negative director. In practice, an excessive mesh refinement may however be needed to create a solid mesh which conforms with the faces of the three-dimensional shell body. In this paper, we shall use the 6-parameter model, but other ways to enable the coupling will be constructed.

We note that we could try to handle coupling conditions by replacing (2) by an augmented energy functional where additional Lagrange multipliers defined on the coupling interface would enter. Here such methods are not straightforward to employ, since after performing the selective dimensional reduction there is no common surface where the Lagrange multipliers could naturally be interpreted as surface forces (tractions). We shall derive methods which do not depend on generating an auxiliary mesh to enforce the coupling.

Preliminaries on conjugate approximations

An account of conjugate approximations given by Brauchli and Oden [2] adds to a theory of finite element approximation concepts which shall be useful for our considerations of calculating coupling constraints and which may be introduced in a manner reminiscent of classical tensor analysis [8]. As a preliminary step, we likewise adopt the summation convention that diagonally twice-repeated indices are summed over their range. In addition, we let $\theta_k \in H^1(\Omega)$ denote standard (Lagrange interpolation) finite element basis functions that allow an approximation $U(\mathbf{x})$ of $u(\mathbf{x})$ over a body Ω as

$$U(\mathbf{x}) = U^k \theta_k(\mathbf{x}). \tag{11}$$

Now, the conjugate basis (or the dual basis in the terminology of tensor analysis adopted in [8]) associated with the set of θ_k is the collection of θ^k obtained by

$$(\theta^k, \theta_i) = \delta_i^k, \tag{12}$$

where $(\cdot, \cdot)$ denotes the $L_2(\Omega)$ inner product and δ_i^k is the Kronecker delta. We may also write $(\cdot, \cdot)_\Omega$ if the domain of integration is made explicit. A conjugate approximation is then defined by

$$U(\mathbf{x}) = U_k \theta^k(\mathbf{x}) = (U, \theta_k)\theta^k(\mathbf{x}). \tag{13}$$

Here the scalars

$$U_k = (U, \theta_k) \tag{14}$$

are referred to as conjugate components, and we also have a similar definition of the component U^k as

$$U^k = (U, \theta^k). \tag{15}$$

We note that concepts which would be similar to those of standard tensor analysis could now be introduced if the metric tensor was replaced by the fundamental (a mass) matrix to "raise and lower" indices. For practical applications, it is important to note that the functions θ^k have a global support, though each of these functions exhibits a decay away from a generating node, whereas the usual finite element basis function θ_k, of course, has a local support.

To get an insight on how conjugate approximations enter into practical finite element computations, we note that given standard abstraction (cf., for example, [3]) of a variational formulation posed over Ω in the form

$$A_\Omega(U, V) = \mathcal{F}_\Omega(V), \tag{16}$$

with $1/2\, A_\Omega(U, U)$ giving the stored energy in terms of a bilinear form $A_\Omega(\cdot, \cdot)$ and with $\mathcal{F}_\Omega(U)$ giving the potential energy of forces, the entries $F_k = \mathcal{F}_\Omega(\theta_k)$ entering the right-hand side vector in the resulting system of linear algebraic equations are not usually thought to have other meanings than discrete forces. However, if the linear functional $\mathcal{F}_\Omega$ can be represented in terms of an input data f as

$$\mathcal{F}_\Omega(V) = (f, V)_\Omega, \tag{17}$$

we have

$$\mathcal{F}_\Omega(\theta_k) = (f, \theta_k)_\Omega = F_k,$$

so that we may reconstruct the data f as the conjugate approximation

$$f(\mathbf{x}) \simeq F_k \theta^k(\mathbf{x}).$$

Although this result is of little consequence in standard computation with a known f, we shall show that an analogue of this computation can be utilized in the derivation of coupling constraints.

Formulation of a coupled model

To introduce in a very simple way how conjugate approximations can be made to enter the formulation of coupled models, we shall first consider the coupling of two three-dimensional models for solids having finite element unknowns $\mathbf{U} : \Omega \to \mathbb{R}^3$ and $\widehat{\mathbf{U}} : \widehat{\Omega} \to \mathbb{R}^3$. Here we assume that the unknown $\widehat{\mathbf{U}}$ obeys a Dirichlet constraint expressed in terms of the values of $\mathbf{U}$ on the coupling interface consisting of the shared boundary $\Gamma \equiv \partial\Omega \cap \partial\widehat{\Omega}$. For simplicity of exposition, we assume that finite element meshes conform on Γ. Although this case seems overly simplistic, the ideas which we shall introduce here are then applied to handle our primary problem of mixed-dimensional coupling between shells and solids.

A variational formulation of the present problem is based on abstractions

$$\begin{aligned} A_\Omega(\mathbf{U}, \mathbf{V}) &= (\mathbf{f}, \mathbf{V})_\Omega + (\mathbf{h}(\widehat{\mathbf{U}}), \mathbf{V})_\Omega, \\ A_{\widehat{\Omega}}(\widehat{\mathbf{U}}, \widehat{\mathbf{V}}) &= (\hat{\mathbf{f}}, \widehat{\mathbf{V}})_{\widehat{\Omega}} + (\mathbf{H}(\widehat{\mathbf{U}}), \widehat{\mathbf{V}})_{\widehat{\Omega}}, \end{aligned} \tag{18}$$

which in essence describe the result of the integration by parts of the inner product of the field equations with a test function defined over each domain. However, the linear functional

$$L_{\widehat{\Omega}}(\widehat{\mathbf{V}}) \equiv (\mathbf{H}(\widehat{\mathbf{U}}), \widehat{\mathbf{V}})_{\widehat{\Omega}} \tag{19}$$

in (18) represents a generalization to reconstruct coupling reactions $\mathbf{H}(\widehat{\mathbf{U}})$ (similar to support reactions as discussed in [4]) when $\widehat{\mathbf{U}}$ is considered to be know and when the treatment of Dirichlet constraints is relaxed somewhat on the coupling interface. In the first place, we must however take $L_{\widehat{\Omega}}(\widehat{\mathbf{V}}) = 0$, since no variations are generally allowed at a boundary associated with Dirichlet constraints.

On the other hand, the linear functional

$$L_\Omega(\mathbf{V}) \equiv (\mathbf{h}(\widehat{\mathbf{U}}), \mathbf{V})_\Omega \tag{20}$$

in (18) is related to the potential energy of the forces exerted on the body Ω by $\widehat{\Omega}$. Its representation will be chosen to depend on how the linear functional $L_{\widehat{\Omega}}$ is constructed. We note that since the linear functional (20) accounts for the coupling forces without referring to surface forces, the first equation of (18) now arises by first integrating by parts under the condition of zero surface force on Γ and then applying the additional coupling forces constructed in the form (20). That we here seek to construct a body force field rather than a surface force field on Γ is a matter of choice.

Now, the standard engineering procedure of computing the discrete coupling reactions (cf., [4]) as

$$\widehat{H}^l_k(\widehat{\mathbf{U}}) = A_{\widehat{\Omega}}(\widehat{\mathbf{U}}, \hat{\theta}_k \mathbf{e}^l) - (\hat{\mathbf{f}}, \hat{\theta}_k \mathbf{e}^l)_{\widehat{\Omega}}, \quad (k, l) \in \mathcal{N}_\Gamma \times \{1, 2, 3\}, \tag{21}$$

where $\mathbf{e}^l = \mathbf{e}_l$ give an orthonormal basis for $\mathbb{R}^3$ and the set $\mathcal{N}_\Gamma$ lists the indices of nodes on Γ, provides us a way to construct the components of the coupling reaction $\mathbf{H} = H^l\mathbf{e}_l$ in the linear functional (19) as conjugate approximations

$$H^l = \widehat{H}^l_k\hat{\theta}^k,$$

as we have

$$\widehat{H}^l_k = L_{\widehat{\Omega}}(\hat{\theta}_k\mathbf{e}^l) = (H^i\mathbf{e}_i, \hat{\theta}_k\mathbf{e}^l)_{\widehat{\Omega}} = (H^l, \hat{\theta}_k)_{\widehat{\Omega}}. \tag{22}$$

On the other hand, using a conjugate approximation for $\mathbf{h}$ in a similar manner gives

$$A_\Omega(\mathbf{U}, \mathbf{V}) = (\mathbf{f}, \mathbf{V})_\Omega + (\theta^k\mathbf{e}_l, \mathbf{V})_\Omega h^l_k, \tag{23}$$

so invoking the law of action and reaction to set

$$h^l_k(\widehat{\mathbf{U}}) = -\widehat{H}^l_k(\widehat{\mathbf{U}}) \tag{24}$$

and using (21) finally give

$$A_\Omega(\mathbf{U}, \mathbf{V}) + \sum_{k\in\mathcal{N}_\Gamma}(\theta^k\mathbf{e}_l, \mathbf{V})_\Omega\, A_{\widehat{\Omega}}(\widehat{\mathbf{U}}, \hat{\theta}_k\mathbf{e}^l) = (\mathbf{f}, \mathbf{V})_\Omega + \sum_{k\in\mathcal{N}_\Gamma}(\theta^k\mathbf{e}_l, \mathbf{V})_\Omega(\hat{\mathbf{f}}, \hat{\theta}_k\mathbf{e}^l)_{\widehat{\Omega}}. \tag{25}$$

We note that the Dirichlet constraints on Γ may be created by requiring that the two linear functionals yielding the values of degrees of freedom associated with the different bodies have equal values for the shared nodes, so that

$$(\widehat{\mathbf{U}}, \hat{\theta}^k\mathbf{e}_l)_{\widehat{\Omega}} = (\mathbf{U}, \theta^k\mathbf{e}_l)_\Omega, \tag{26}$$

giving

$$\widehat{U}^k_l = (\mathbf{U}, \theta^k\mathbf{e}_l)_\Omega \tag{27}$$

or, simply,

$$\widehat{U}^k_l = U^k_l, \tag{28}$$

where $(k, l) \in \mathcal{N}_\Gamma \times \{1, 2, 3\}$. In view of the foregoing considerations, the variational formulation of the coupled problem can now be put into the form (here the construction of H^1-regular finite element spaces is standard and we omit the details): Find $(\mathbf{U}, \widehat{\mathbf{U}}) \in \mathbf{X} \times \widehat{\mathbf{X}}$ such that

$$\begin{aligned} A_\Omega(\mathbf{U}, \mathbf{V}) + \sum_{k\in\mathcal{N}_\Gamma}(\theta^k\mathbf{e}_l, \mathbf{V})_\Omega\, A_{\widehat{\Omega}}(\widehat{\mathbf{U}}, \hat{\theta}_k\mathbf{e}^l) &= (\mathbf{f}, \mathbf{V})_\Omega + \sum_{k\in\mathcal{N}_\Gamma}(\theta^k\mathbf{e}_l, \mathbf{V})_\Omega(\hat{\mathbf{f}}, \hat{\theta}_k\mathbf{e}^l)_{\widehat{\Omega}}, \\ A_{\widehat{\Omega}}(\widehat{\mathbf{U}}, \widehat{\mathbf{V}}) &= (\hat{\mathbf{f}}, \widehat{\mathbf{V}})_{\widehat{\Omega}}, \\ (\mathbf{U}, \theta^i\mathbf{e}_j)_\Omega - \widehat{U}^i_j &= 0 \end{aligned} \tag{29}$$

for all kinematically admissible test functions $(\mathbf{V}, \widehat{\mathbf{V}}) \in \mathbf{X}_{\partial\Omega_D} \times \widehat{\mathbf{X}}_{\partial\widehat{\Omega}_D}$, and $(i, j) \in \mathcal{N}_\Gamma \times \{1, 2, 3\}$. The repeated occurrence of the scalar coefficients of the form $(\theta^k\mathbf{e}_l, \mathbf{V})_\Omega$ both in the terms that account for the coupling forces and in the Dirichlet constraints is notable.

A characteristic property of our formulation is work equilibration, i.e., for the solution of the coupled problem we have

$$(\mathbf{h}(\widehat{\mathbf{U}}), \mathbf{U})_\Omega + (\mathbf{H}(\widehat{\mathbf{U}}), \widehat{\mathbf{U}})_{\widehat{\Omega}} = 0, \tag{30}$$

which can be verified easily. It is notable that our procedure does not make any reference to a traction field on the surface Γ. This is a consequence of our choice to reconstruct a coupling body force field rather than a surface force field on Γ.

Model for shell-solid coupling

We now try to imitate the development above in the case of shell-solid interaction. The unknown of the shell model is a finite element field $\widehat{\mathbf{U}} \equiv (\hat{\mathbf{v}}, \hat{\boldsymbol{\beta}}) : \omega \to \mathbb{R}^3 \times \mathbb{R}^3$, and the variational formulation of this model is now based on abstraction

$$A_\omega(\widehat{\mathbf{U}}, (\widehat{\mathbf{w}}, \hat{\boldsymbol{\eta}})) = (\hat{\mathbf{g}}, (\widehat{\mathbf{w}}, \hat{\boldsymbol{\eta}}))_\omega + L_\omega((\widehat{\mathbf{w}}, \hat{\boldsymbol{\eta}})), \tag{31}$$

where the linear functional L_ω to construct coupling reactions splits up into two parts as

$$L_\omega((\widehat{\mathbf{w}}, \hat{\boldsymbol{\eta}})) = (\mathbf{H}(\widehat{\mathbf{U}}), \widehat{\mathbf{w}})_\omega + (\boldsymbol{\Lambda}(\widehat{\mathbf{U}}), \hat{\boldsymbol{\eta}})_\omega, \tag{32}$$

with $\mathbf{H}(\widehat{\mathbf{U}})$ and $\boldsymbol{\Lambda}(\widehat{\mathbf{U}})$ interpreted as force resultants. As constraints of Dirichlet type which enforce the shell to follow the displacement $\mathbf{U} : \Omega \to \mathbb{R}^3$ of the solid, we employ

$$\begin{aligned} (\hat{\mathbf{v}}, \hat{\theta}^k \mathbf{e}_l)_\omega &= (\mathbf{U}, \theta^k \mathbf{e}_l)_\Omega, \\ (\hat{\boldsymbol{\beta}}, \hat{\theta}^k \mathbf{e}_l)_\omega &= -(D\mathbf{U}[\boldsymbol{d}], \theta^k \mathbf{e}_l)_\Omega, \end{aligned} \tag{33}$$

which are analogous to (26). Here mesh conformity is again supposed, so that any shell edge which is a part of the (now, one-dimensional) coupling interface Γ is also an edge of a solid element.

On the other hand, the abstraction to represent the variational formulation for the solid is here augmented as

$$A_\Omega(\mathbf{U}, \mathbf{V}) = (\mathbf{f}, \mathbf{V})_\Omega + (\mathbf{h}(\widehat{\mathbf{U}}), \mathbf{V})_\Omega - (\boldsymbol{\lambda}(\widehat{\mathbf{U}}), D\mathbf{V}[\boldsymbol{d}])_\Omega, \tag{34}$$

where the form of the last term is chosen such that it enables the development of the idea of work equilibration. In this case, we can compute the discrete coupling reactions by

$$\begin{aligned} \widehat{H}^l_k(\widehat{\mathbf{U}}) &= L_\omega((\hat{\theta}_k \mathbf{e}^l, \mathbf{0})) = A_\omega(\widehat{\mathbf{U}}, (\hat{\theta}_k \mathbf{e}^l, \mathbf{0})) - (\hat{\mathbf{g}}, (\hat{\theta}_k \mathbf{e}^l, \mathbf{0}))_\omega, \\ \hat{\Lambda}^l_k(\widehat{\mathbf{U}}) &= L_\omega((\mathbf{0}, \hat{\theta}_k \mathbf{e}^l)) = A_\omega(\widehat{\mathbf{U}}, (\mathbf{0}, \hat{\theta}_k \mathbf{e}^l)) - (\hat{\mathbf{g}}, (\mathbf{0}, \hat{\theta}_k \mathbf{e}^l))_\omega, \end{aligned} \tag{35}$$

with $(k, l) \in \mathcal{N}_\Gamma \times \{1, 2, 3\}$, so that the conjugate approximations $\mathbf{H} = \mathbf{e}_l \widehat{H}^l_k \hat{\theta}^k$ and $\boldsymbol{\Lambda} = \mathbf{e}_l \hat{\Lambda}^l_k \hat{\theta}^k$ can be obtained. If we assume analogous expansions for $\mathbf{h}$ and $\boldsymbol{\lambda}$ together with setting

$$\begin{aligned} h^l_k(\widehat{\mathbf{U}}) &= -\widehat{H}^l_k(\widehat{\mathbf{U}}), \\ \lambda^l_k(\widehat{\mathbf{U}}) &= -\hat{\Lambda}^l_k(\widehat{\mathbf{U}}), \end{aligned} \tag{36}$$

we are able to present the variational formulation of the coupled problem in the form: Find $(\mathbf{U}, \widehat{\mathbf{U}}) \in \mathbf{X} \times \mathbf{Z}$ such that

$$\begin{aligned} A_\Omega(\mathbf{U}, \mathbf{V}) + \sum_{k \in \mathcal{N}_\Gamma} (\theta^k \mathbf{e}_l, \mathbf{V})_\Omega \, A_\omega(\widehat{\mathbf{U}}, (\hat{\theta}_k \mathbf{e}^l, \mathbf{0})) - \\ \sum_{k \in \mathcal{N}_\Gamma} (\theta^k \mathbf{e}_l, D\mathbf{V}[\boldsymbol{d}])_\Omega \, A_\omega(\widehat{\mathbf{U}}, (\mathbf{0}, \hat{\theta}_k \mathbf{e}^l)) = (\mathbf{f}, \mathbf{V})_\Omega + \sum_{k \in \mathcal{N}_\Gamma} (\theta^k \mathbf{e}_l, \mathbf{V})_\Omega \, (\hat{\mathbf{g}}, (\hat{\theta}_k \mathbf{e}^l, \mathbf{0}))_\omega - \\ \sum_{k \in \mathcal{N}_\Gamma} (\theta^k \mathbf{e}_l, D\mathbf{V}[\boldsymbol{d}])_\Omega \, (\hat{\mathbf{g}}, (\mathbf{0}, \hat{\theta}_k \mathbf{e}^l))_\omega, \\ A_\omega(\widehat{\mathbf{U}}, \widehat{\mathbf{V}}) = (\hat{\mathbf{g}}, \widehat{\mathbf{V}})_\omega, \\ (\mathbf{U}, \theta^i \mathbf{e}_j)_\Omega - (\hat{\mathbf{v}}, \hat{\theta}^i \mathbf{e}_j)_\omega = 0, \\ (D\mathbf{U}[\boldsymbol{d}], \theta^i \mathbf{e}_j)_\Omega + (\hat{\boldsymbol{\beta}}, \hat{\theta}^i \mathbf{e}_j)_\omega = 0 \end{aligned} \tag{37}$$

for all kinematically admissible test functions $(\mathbf{V}, \widehat{\mathbf{V}}) \in \mathbf{X}_{\partial\Omega_D} \times \mathbf{Z}_{\partial\omega_D}$ and $(i,j) \in \mathcal{N}_\Gamma \times \{1,2,3\}$.

We conclude this development by stating an energy result related to our variational formulation of the coupled problem.

Proposition (work equilibration). *Let* $\mathbf{U} : \Omega \to \mathbb{R}^3$ *and* $\widehat{\mathbf{U}} \equiv (\hat{\mathbf{v}}, \hat{\boldsymbol{\beta}}) : \omega \to \mathbb{R}^3 \times \mathbb{R}^3$ *be the solution pair of the coupled problem defined by the variational formulation (37) and let*

$$L_\omega(\cdot) = A_\omega(\widehat{\mathbf{U}}, \cdot) - (\hat{\mathbf{g}}, \cdot)_\omega$$

be the linear functional to construct the coupling reactions exerted on the shell, so that it can be expressed as

$$L_\omega((\widehat{\mathbf{w}}, \hat{\boldsymbol{\eta}})) = (\mathbf{e}_l \widehat{H}^l_k(\widehat{\mathbf{U}})\hat{\theta}^k, \widehat{\mathbf{w}})_\omega + (\mathbf{e}_l \hat{\Lambda}^l_k(\widehat{\mathbf{U}})\hat{\theta}^k, \hat{\boldsymbol{\eta}})_\omega,$$

with the conjugate components $\widehat{H}^l_k(\widehat{\mathbf{U}})$ *and* $\hat{\Lambda}^l_k(\widehat{\mathbf{U}})$ *defined by (35). Then the potential energy of the forces exerted on the solid, which is defined by*

$$(\mathbf{h}(\widehat{\mathbf{U}}), \mathbf{U})_\Omega - (\boldsymbol{\lambda}(\widehat{\mathbf{U}}), D\mathbf{U}[\boldsymbol{d}])_\Omega = (\mathbf{e}_l h^l_k(\widehat{\mathbf{U}})\theta^k, \mathbf{U})_\Omega - (\mathbf{e}_l \lambda^l_k(\widehat{\mathbf{U}})\theta^k, D\mathbf{U}[\boldsymbol{d}])_\Omega,$$

and the potential energy of the coupling reactions given by $L_\omega(\widehat{\mathbf{U}})$ *satisfy*

$$L_\omega(\widehat{\mathbf{U}}) + (\mathbf{h}(\widehat{\mathbf{U}}), \mathbf{U})_\Omega - (\boldsymbol{\lambda}(\widehat{\mathbf{U}}), D\mathbf{U}[\boldsymbol{d}])_\Omega = 0. \tag{38}$$

This result can be verified easily, as we obtain

$$\begin{aligned} L_\omega(\widehat{\mathbf{U}}) + (\mathbf{h}(\widehat{\mathbf{U}}), \mathbf{U})_\Omega - (\boldsymbol{\lambda}(\widehat{\mathbf{U}}), D\mathbf{U}[\boldsymbol{d}])_\Omega =& \widehat{H}^j_k(\widehat{\mathbf{U}})\hat{v}^k_j + \hat{\Lambda}^j_k(\widehat{\mathbf{U}})\hat{\beta}^k_j + h^j_k(\widehat{\mathbf{U}})U^k_j - \\ & \lambda^j_k(\widehat{\mathbf{U}})(D\mathbf{U}[\boldsymbol{d}], \theta^k \mathbf{e}_j)_\Omega, \end{aligned} \tag{39}$$

so that invoking the conditions (33) and (36) that are included in (37) gives the desired result. The above proposition yields corollary that when the Dirichlet constraints on $\partial\Omega_D$ and $\partial\omega_D$ are homogeneous (note that a problem with nonhomogeneous constraints can easily be transformed to a problem with homogeneous conditions), the potential energy of the external forces

$$\mathcal{F}\{\mathbf{U}, \hat{\mathbf{U}}\} \equiv (\mathbf{f}, \mathbf{U})_\Omega + (\hat{\mathbf{g}}, \widehat{\mathbf{U}})_\omega$$

is twice the total stored energy in the structure, since, in view of (31) and (34), we have

$$\begin{aligned} A_\Omega(\mathbf{U}, \mathbf{U}) + A_\omega(\widehat{\mathbf{U}}, \widehat{\mathbf{U}}) &= (\mathbf{f}, \mathbf{U})_\Omega + (\mathbf{h}(\widehat{\mathbf{U}}), \mathbf{U})_\Omega - (\boldsymbol{\lambda}(\widehat{\mathbf{U}}), D\mathbf{U}[\boldsymbol{d}])_\Omega + (\hat{\mathbf{g}}, \widehat{\mathbf{U}})_\omega + L_\omega(\widehat{\mathbf{U}}) \\ &= \mathcal{F}\{\mathbf{U}, \hat{\mathbf{U}}\}. \end{aligned} \tag{40}$$

That is, no perturbation of energy is associated with the coupling forces.

Implementation within Elmer software

The coupled model based on the formulation (37) has been implemented into open source FEM software Elmer [10] in the case of certain lowest-order shell finite elements. In general, Elmer is designed to handle multiphysics problems, with possibilities to couple a large variety of physical models of different disciplines. The coupling is usually done by

using a loosely coupled iteration scheme where each physical model is solved repeatedly, with updated coupling conditions. This approach supports software modularity in a natural way, but sometimes attaining convergence may be problematic. Instead, treating all constituent models simultaneously is well suited for problems where physical couplings are especially strong, but this strategy is more demanding to implement, requiring additional flexibility of software. Gradual efforts have been made to support a better construction of such models within Elmer. The procedure to create the coupled model based on the formulation (37) also utilizes this more recent work on building tightly coupled solvers.

Given the ability to compute the structural equations for solids and shells in their own domains of definition, together with a procedure to calculate the scalar coefficients of the form

$$(\theta^k \mathbf{e}_l, D\mathbf{V}[\boldsymbol{d}])_\Omega, \tag{41}$$

the discrete model based on (37) can be assembled by accessing the entries of the matrices and the right-hand side vectors which are associated with the constituent models and needed even when the coupling of the models is not enforced. In this case, we need to assemble the algebraic system of equations having the natural block structure

$$\begin{bmatrix} \mathbf{K} & \mathbf{N} \\ \mathbf{D} & \mathbf{A} \end{bmatrix} \begin{bmatrix} \mathbf{U} \\ \hat{\mathbf{U}} \end{bmatrix} = \begin{bmatrix} \mathbf{F} \\ \mathbf{G} \end{bmatrix}, \tag{42}$$

where $\mathbf{K}$ and $\mathbf{A}$ are the stiffness matrices associated with the solid and the shell, respectively. Elmer now provides general utilities for the flexible creation of a block matrix structure and an associated right-hand side vector, so that pointers to the entries of $\mathbf{K}$ and $\mathbf{A}$ can be used when the system (42) is created. On the other hand, a special subroutine is used to add the coupling blocks $\mathbf{N}$ and $\mathbf{D}$ in (42).

Our way to enforce the Dirichlet constraints on the coupling interface Γ is based on assembling matrix rows having just two entries, with either of them being a diagonal entry, so that $\mathbf{A}$ contains a diagonal part. Before this is done, these rows of $\mathbf{A}$ are defined to have the entries which would be appropriate if non-vanishing test functions associated with Γ were allowed. Prior to rewriting to obtain the diagonal part of $\mathbf{A}$, the weighted versions of these entries are calculated in order to insert the suitable entries into $\mathbf{N}$.

To handle problems including the inertial body force $-\rho\ddot{\boldsymbol{u}}$, with ρ a density field, the mass matrix of the coupled model can analogously be assembled in the block matrix form

$$\begin{bmatrix} \mathbf{M}_{KK} & \mathbf{M}_{KA} \\ \mathbf{0} & \mathbf{M}_{AA} \end{bmatrix}. \tag{43}$$

Again, the mass matrix $\mathbf{M}_{AA}$ for the shell equations is originally computed such that it would be appropriate if non-vanishing test functions associated with the coupling interface Γ were allowed. When suitable continuity constraints on the inertial force terms based on the conditions (33) are set, the shell mass matrix entries in the rows corresponding to the nodes on Γ are used to create the coupling block $\mathbf{M}_{KA}$. After this has been done, these rows of $\mathbf{M}_{AA}$ are rewritten to have zero entries, so that the coupling constraints of Dirichlet type can be respected in the end.

In order to enable flexible use of linear solvers, the block matrix construct used within Elmer to represent the coefficient matrices and vectors in (42) and (43) can be converted to the usual CRS matrix format. This causes some overhead, but no adaptations of code are then necessary to employ existing interfaces for libraries that offer linear solvers or

methods for eigenvalue problems. In addition, the computation of algebraic preconditioners, such as incomplete LU factorizations, can be performed in the usual way. On the other hand, if the special block matrix construct is maintained, Elmer can also use splitting strategies (cf., [1]) based on the block structure to perform the iterative solution of the coupled system of linear algebraic equations. This approach may enable the development of iterative solvers where highly efficient methods such as multigrid algorithms designed for the constituent models are reused in the solution of the coupled model.

The remaining technicalities are related to ways to estimate the scalar coefficients of the type (41) which depend on the conjugate basis functions associated with the indices in $\mathcal{N}_\Gamma$. A practical method to obtain these approximations would be to perform several iterative solutions of linear systems, with the coefficient matrix being the fundamental matrix of the solid discretization and with a suitable collection of right-hand side vectors. However, the current implementation within Elmer does not employ such global approximations, but averaging is applied to compute constraints which allow for the direct elimination of the unknowns $\hat{\beta}_j^i$ on Γ in a similar way as the formulation (37) does. We then conjecture that the resulting coefficients can be used as the estimates of the values (41).

We note that Elmer can automatically generate the coupling interface Γ by using the assumption that any shell edge $\mathcal{E}_e \subset \Gamma$ is also an edge of a solid element. In the first place the unknown $\hat{\boldsymbol{\beta}}$ is tied at the centre of $\mathcal{E}_e$, but assuming a constant approximation of $\hat{\boldsymbol{\beta}}$ on $\mathcal{E}_e$ gives two constraints of a similar content for the nodes that define $\mathcal{E}_e$. Each element in a set $\mathcal{K}_e$ of solid elements having $\mathcal{E}_e$ as an edge contributes to the nodal constraint as

$$\alpha^k \hat{\beta}_i^k = \frac{1}{M_k} \sum_{j=1}^{E} g^j, \tag{44}$$

where g^j are different elementwise approximations of the ith component of the directional derivative, M_k is the count of nodal constraint updates after looping over all elements in the set $\mathcal{K}_e$ of the cardinality E, and an additional weight α^k ensures that the weights sum up to the unity after assembling the constraints associated with all the edges $\mathcal{E}_e \subset \Gamma$. An additional level of averaging is also possible if several shell elements share a coupling interface edge.

Examples

To demonstrate the utility of the coupling procedure presented in this paper, we now use the implementation available in Elmer to solve a coupled model of a straight cylindrical shell. We note that the development of coupling schemes which give accurate results for deformations dominated by bending effects is in general less obvious. We therefore consider a problem where the entire shell is constrained by conditions which only prevent rigid body motions, so that bending-dominated deformations are possible [3].

Here a boundary layer adjacent to a free edge is modelled by using a standard lowest-order approximation based on hexahedral finite elements, whereas elsewhere we use four-node shell finite elements, with special strain reduction operators in order to alleviate locking. For verification purposes we also solve the same problem by using either only shell finite elements or only solid finite elements. In order to roughly estimate the errors of the lowest-order models, we shall also employ solid finite elements of degree $p = 2$. We note that a severe locking would be expected if the problem was modelled by using standard lowest-order finite elements of a characteristic size larger than the shell thickness.

The shell thickness d is taken to be a parameter, whereas the length and the radius of the shell are taken to be $L = 2$ and $R = 1$, respectively. A dimensionless thickness is defined by $t = d/R$. The material properties are characterized by Poisson's ratio $\nu = 1/3$, Young's modulus $E = 7.0 \cdot 10^{10}$, and the density $\rho = 2700$. Eigenanalysis is then performed by seeking only symmetric modes over a mesh representing an eighth of the whole structure.

In the case of the coupled model, the solid mesh is confined to a layer of length $\delta = 2d$, so that the shortest boundary layers of characteristic length $\ell \sim d$ are mainly resolved over the solid mesh, while the boundary layers of characteristic length $\ell \sim \sqrt{dR}$ also extend over the surface mesh. For the layer a hexahedral $(32 \times 32 \times 4)$-mesh is generated, with four layers of elements used over the thickness, while outside this region a quadrilateral (32×32)-mesh is used. In the case of a pure discretization with the shell finite elements, a similar mesh without the selective mesh extrusion over the thickness is used. On the other hand, in the case of a pure discretization with the solid finite elements the mesh extrusion is done over the whole computational domain. The mesh size parameter h is the same for the solid discretization of degree $p = 2$, but additional degrees of freedom are then created by associating them with the sets of edges, faces and element interiors of the lowest-order $(p = 1)$ mesh.

We note that since the standard lowest-order solid finite elements are used and since the mesh resolution is not altered when the shell thickness is varied, the accuracy of the solid discretization is expected to deteriorate as the shell thickness decreases. Although the boundary layer mesh has a fine resolution in the axial direction to capture the exponentially decaying boundary layers, this failure affects also the coupled model, since all the models share the same mesh resolution in the angular direction. Therefore, we shall focus on the cases where $d \geq 0.05$, so that the mesh size parameter h satisfies $h/d = O(1)$ with respect to the variations of d. Hence, our three-dimensional discretizations should not suffer severe locking. On the other hand, our discrete shell model would not need such constraint on the mesh size, i.e., its behavior should be more robust as $t \to 0$.

To begin with, Table 1 shows the eigenvalues obtained by using the different models when $t = 0.1$. It is noted that the eigenvalues of two models of different types cannot be expected to converge to the same result when the discretizations are refined and the thickness is kept fixed, but relatively close approximations may anyhow be expected. It should also be noted that the comparison of the results requires some care as the comparison of the kth eigenvalues (as listed in the ascending order) may lead to comparing the eigenvectors which do not approximate the same characteristic mode. To avoid such discrepancies, a visual inspection of the eigenvectors was done in order to list the eigenvalues so that the agreement with the characteristic modes of the second-order solid model is obtained. Therefore, the list of eigenvalues for a specific model may not follow the ascending order, but we shall make these exceptions clear in our discussion. We also note that in all computations the assembly of the coupling block $\mathbf{M}_{KA}$ of the mass matrix was simplified by neglecting the inertial effects associated with the approximation $\hat{\boldsymbol{\beta}}$ on the coupling interface Γ.

Table 1 shows that the eigenvalues of the pure shell model are notably close to those of the second-order solid model, the average of the relative difference between the eigenvalues being only 0.91%. The same average difference computed for the lowest-order solid model is 5.4%. In this case the reordering of the eigenvalues was done, so we thus consider the approximations $\lambda_7^{p=2} \approx \lambda_6^{p=1}$ and $\lambda_6^{p=2} \approx \lambda_7^{p=1}$, where the index of the eigenvalue is according to the original ascending order. The coupled model also needs the similar

Table 1. Eigenvalues for the different models of a cylinder of thickness $t = 0.1$.

Mode	Coupled model	Shell	Solid p=1	Solid p=2
1	$1.7172 \cdot 10^5$	$1.6878 \cdot 10^5$	$1.8596 \cdot 10^5$	$1.6844 \cdot 10^5$
2	$4.9018 \cdot 10^6$	$4.8108 \cdot 10^6$	$5.2819 \cdot 10^6$	$4.7559 \cdot 10^6$
3	$1.1393 \cdot 10^7$	$1.1704 \cdot 10^7$	$1.1817 \cdot 10^7$	$1.1711 \cdot 10^7$
4	$1.2471 \cdot 10^7$	$1.2499 \cdot 10^7$	$1.2996 \cdot 10^7$	$1.2362 \cdot 10^7$
5	$2.4327 \cdot 10^7$	$2.4337 \cdot 10^7$	$2.4370 \cdot 10^7$	$2.4351 \cdot 10^7$
6	$2.6373 \cdot 10^7$	$2.5882 \cdot 10^7$	$2.8254 \cdot 10^7$	$2.5195 \cdot 10^7$
7	$2.6295 \cdot 10^7$	$2.6271 \cdot 10^7$	$2.6366 \cdot 10^7$	$2.6287 \cdot 10^7$
8	$3.9042 \cdot 10^7$	$3.8666 \cdot 10^7$	$4.0920 \cdot 10^7$	$3.7685 \cdot 10^7$
9	$4.3954 \cdot 10^7$	$4.4741 \cdot 10^7$	$4.5695 \cdot 10^7$	$4.4542 \cdot 10^7$
10	$4.4233 \cdot 10^7$	$4.5628 \cdot 10^7$	$4.6653 \cdot 10^7$	$4.5339 \cdot 10^7$

Table 2. Eigenvalues for the different models of a cylinder of thickness $t = 0.05$.

Mode	Coupled model	Shell	Solid p=1	Solid p=2
1	$4.4388 \cdot 10^4$	$4.2929 \cdot 10^4$	$5.7782 \cdot 10^4$	$4.2797 \cdot 10^4$
2	$1.3034 \cdot 10^6$	$1.2564 \cdot 10^6$	$1.6889 \cdot 10^6$	$1.2438 \cdot 10^6$
3	$4.8747 \cdot 10^6$	$4.7902 \cdot 10^6$	$5.2599 \cdot 10^6$	$4.7436 \cdot 10^6$
4	$7.3200 \cdot 10^6$	$7.0394 \cdot 10^6$	$9.4319 \cdot 10^6$	$6.8852 \cdot 10^6$
5	$1.0313 \cdot 10^7$	$1.0356 \cdot 10^7$	$1.0453 \cdot 10^7$	$1.0350 \cdot 10^7$
6	$1.1689 \cdot 10^7$	$1.1149 \cdot 10^7$	$1.3541 \cdot 10^7$	$1.0917 \cdot 10^7$
7	$2.3838 \cdot 10^7$	$2.2969 \cdot 10^7$	$3.0639 \cdot 10^7$	$2.2100 \cdot 10^7$
8	$2.4288 \cdot 10^7$	$2.4289 \cdot 10^7$	$2.4320 \cdot 10^7$	$2.4297 \cdot 10^7$
9	$2.4608 \cdot 10^7$	$2.4788 \cdot 10^7$	$2.6414 \cdot 10^7$	$2.4638 \cdot 10^7$
10	$2.5951 \cdot 10^7$	$2.5939 \cdot 10^7$	$2.6034 \cdot 10^7$	$2.5956 \cdot 10^7$

reordering and gives 2.1% as the average relative difference between the eigenvalues.

The similar results for the shell thickness $t = 0.05$ are given in Table 2. Now the average relative difference between the eigenvalues of the second-order solid model and those of the pure shell model is found to be 1.1%. The pure solid model of the lowest order starts to show the growth of errors (that is, the symptoms of locking) as the average relative difference between the eigenvalues is already 19.0%. In this case, the reordering of the eigenvalues was done, so that the approximations $\lambda_7^{p=2} \approx \lambda_{11}^{p=1}$, $\lambda_8^{p=2} \approx \lambda_7^{p=1}$, and $\lambda_{10}^{p=2} \approx \lambda_8^{p=1}$ are considered. Here the eigenvalue index is again according to the original ascending order. We however see that all the eigenvalues of the coupled model are in reasonable agreement with those of the second-order solid model even for the smaller thickness $t = 0.05$, the average relative difference between the eigenvalues being 3.3%. The eigenmodes computed also exhibit good visual agreement, which is illustrated in Figure 1 by comparing the 2-norms of the displacement vectors in the case of the sixth mode.

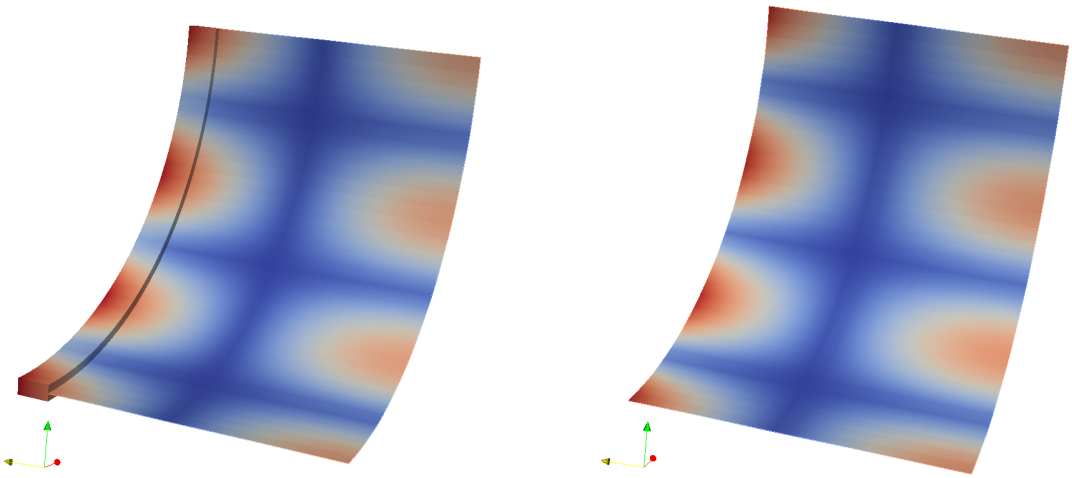

Figure 1. The 2-norm of the displacement vector for the sixth mode obtained for the thickness $t = 0.05$ with the coupled model (the eigenvalue $\lambda_6 \approx 1.1689 \cdot 10^7$) and the pure shell model ($\lambda_6 \approx 1.1149 \cdot 10^7$).

A closer inspection of the results revealed that the eigenvalues tend to be more inaccurate for the eigenmodes which are characterized by oscillations in the angular direction. In addition, even for the thickness $t = 0.1$, some eigenvalues of the lowest-order solid model are seen to have relatively large errors. It thus appears that the strain reduction operators used in the discrete shell model are beneficial even for a relatively thick shell. We shall next make a closer look at how the coupled model can handle possibly unbalanced numerical approximation errors of the constituent models. As representative cases we consider the approximations of the first and fifth eigenmodes for which the relative differences between the respective eigenvalues of the solid models of different degree are 10.4% and 0.079%, respectively. The fifth eigenmode is characterized by an axially changing deformation, while the first eigenmode has the minimal number of smooth oscillations in the angular direction, has a notable boundary layer and is also observed to be increasingly bending-dominated when the thickness decreases.

Figures 2 and 3 illustrate axial profiles of the axial and transverse displacements, together with the axial and transverse components of the directional displacement derivative in the direction of the negative director, obtained for the representative modes ($t = 0.1$) by the pure shell model, the coupled model, and the pure solid model of the lowest degree. The profiles are shown along the segment which lies on the mid-surface and which intersects a model boundary where the symmetry conditions are imposed. In the case of approximation over a solid mesh, the directional derivative is computed as the first order divided difference of the displacement by using the nodes which are at equal distances $d/4 = 0.025$ from the mid-surface. That is, we use a more localized approximation as compared with the two-dimensional shell theory, where considering the difference of the displacements of the surface points at equal distances $d/2$ from the mid-surface is more natural.

We first note that in the case of the fifth mode the solutions of the pure shell model

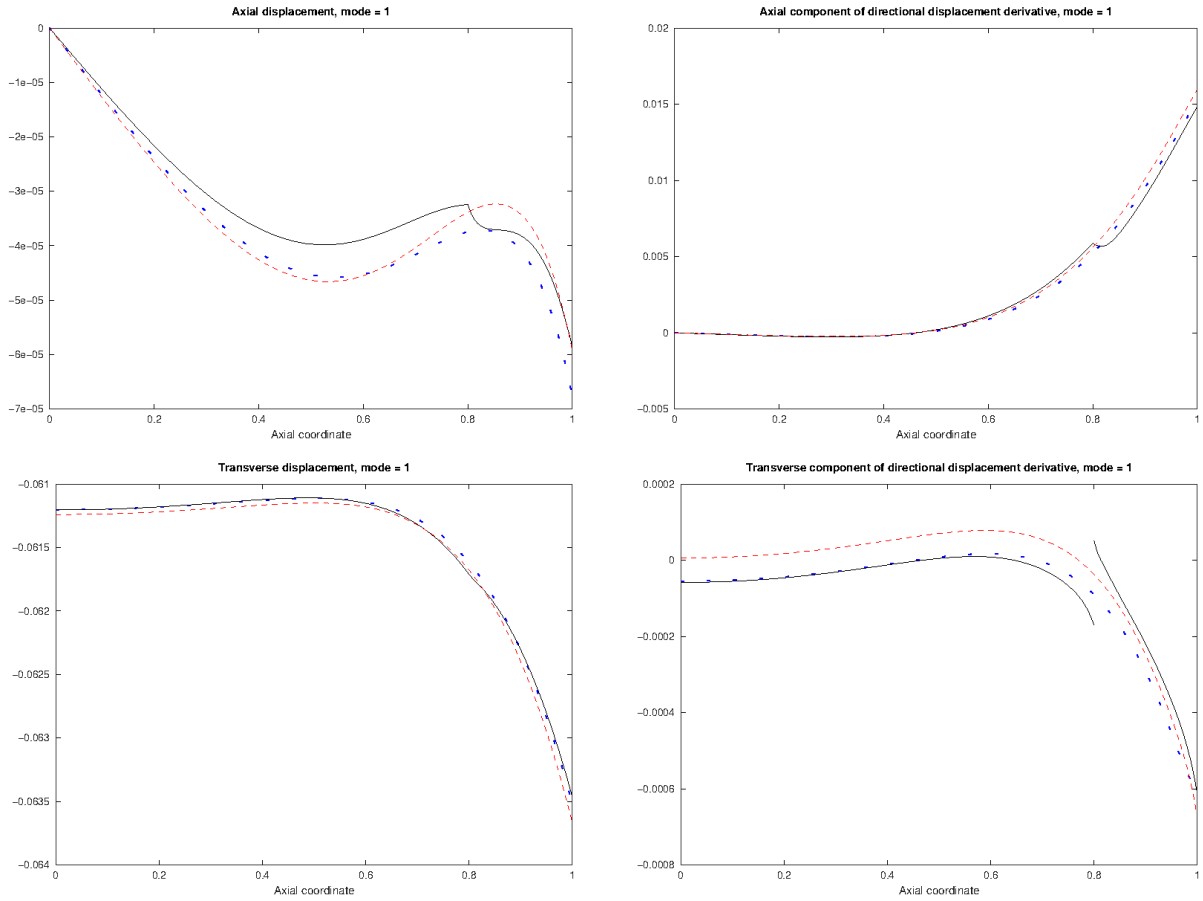

Figure 2. The profiles of the axial and transverse displacements, together with the axial and transverse components of the directional displacement derivative in the direction of the negative director, for the first eigenmode ($t = 0.1$) given by the pure shell model (dotted lines), the coupled model (solid lines), and the pure solid model of the lowest degree (dashes lines).

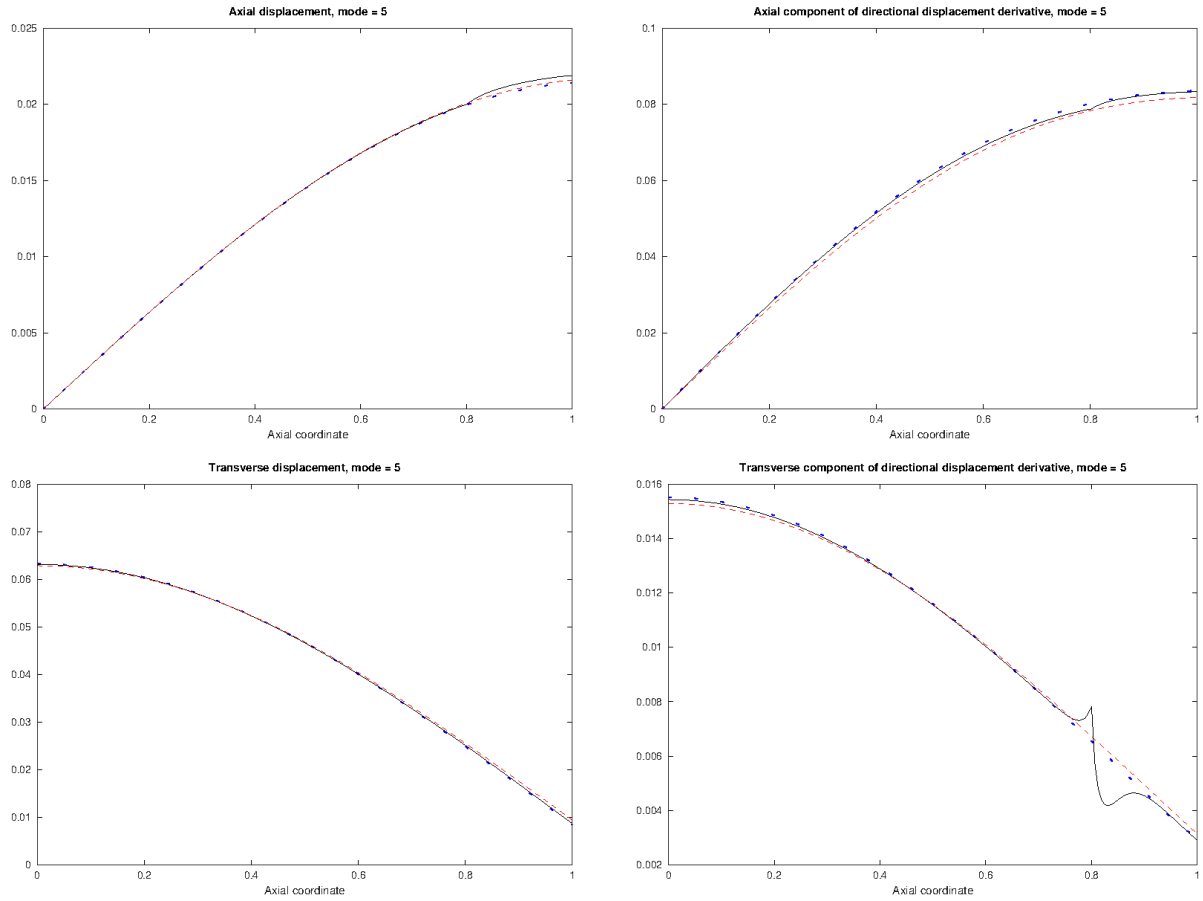

Figure 3. The profiles of the axial and transverse displacements, together with the axial and transverse components of the directional displacement derivative in the direction of the negative director, for the fifth eigenmode ($t = 0.1$) given by the pure shell model (dotted lines), the coupled model (solid lines), and the pure solid model of the lowest degree (dashes lines).

and the pure solid model are close to each other, whereas the axial displacement and the transverse component of the directional displacement derivative (the negative of the transverse normal strain) obtained for the first mode have notable differences. These discrepancies, which also occur at the point corresponding to coupling interface (the axial coordinate value $z = 0.8$), give a likely explanation for the clear imperfections which are seen in the first eigenmode of the coupled model. Overall, in spite of its discontinuity, the transverse normal strain of the coupled model is closer to that given by the pure shell model, whose eigenvalue differs from that of the second-order solid model only by 0.2%. In the case of the coupled model this relative difference is 1.9%, which should be compared with the corresponding difference 10.4% of the pure solid model. On the other hand, in the case of the fifth mode we see a significant discrepancy only in the transverse normal strain. This imperfection seems to be a local effect decaying in the length scale $\sim d$. Nevertheless, all the models give very close approximations of the fifth eigenvalue obtained by the second-order solid model.

A satisfactory explanation for the higher sensitivity of the coupled approximation of transverse normal strain seen in the above examples is left as an open question. We however mention that our local approximations to avoid the global computation of the conjugate basis functions might cause some effects. Some discrepancies might also originate from shell theories. In particular, the development of transverse shear strains resulting from (6) under the constraint (7) is not complete, since both the neglected tangential components of $\boldsymbol{\psi}$ and the tangential derivatives of the component $\boldsymbol{\beta} \cdot \boldsymbol{a}_3$, which equals the negative of the transverse normal strain, contribute to the first-order terms of transverse shear strains in the thickness coordinate y^3. Thus, the shell model we have employed may not be able to give a sufficient description of transverse shear deformations occurring over the shortest $O(t)$ scales. In addition, some effects might also originate from our simplified implementation of the shell model which is best fitted for cases $t \ll 1$, the variational formulation being simplified by neglecting $O(t)$ terms.

The above examples represent cases where the solid part is added in order to fully account for three-dimensional effects in a boundary layer. These examples clearly demonstrate that such simulations require special three-dimensional discretizations which can alleviate effects of locking related to thin bodies. Otherwise, unbalanced numerical approximation errors of the constituent models are to be expected, possibly leading to imperfections, although the shell might be so thick that severe locking is not an issue. To conclude, we finally consider a model which represents another problem of interest where a relatively thick solid is coupled with a shell of smaller thickness. In such cases the use of the standard low-order solid finite elements is generally a more realistic option. Our coupled model is similar to that for the shell thickness $t = 0.1$, but we now decrease the shell thickness over the surface model to the value $t = 0.05$, so that the solid part acts as a stiffener. The eigenvalues of this model are given in Table 3 and they may be compared with the eigenvalues given in Tables 1 and 2. The stiffening effect is also illustrated in Figure 4 where we compare the second eigenmode obtained when the cylinder is of uniform thickness $t = 0.05$ (the eigenvalue $\lambda_2 \approx 1.2564 \cdot 10^6$) and when it has the stiffener ($\lambda_2 \approx 2.0639 \cdot 10^6$).

Concluding remarks

Our method for mixed-dimensional coupling between shells and solids presented in this paper is surprisingly simple, as it does not depend on additional computational parame-

Table 3. Eigenvalues for the coupled model of a cylinder of thickness $t = 0.05$ with a stiffener ring of thickness $t = 0.1$.

Mode	Eigenvalue
1	$8.6201 \cdot 10^4$
2	$2.0639 \cdot 10^6$
3	$6.4936 \cdot 10^6$
4	$8.5849 \cdot 10^6$
5	$8.8810 \cdot 10^6$
6	$2.1340 \cdot 10^7$
7	$2.3283 \cdot 10^7$
8	$2.5889 \cdot 10^7$
9	$2.6212 \cdot 10^7$
10	$2.7894 \cdot 10^7$

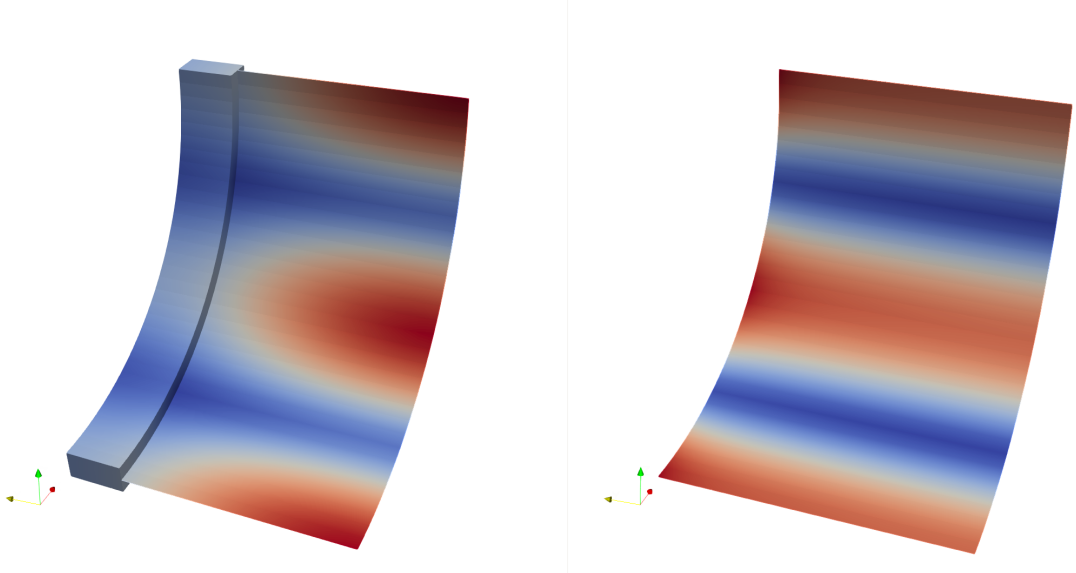

Figure 4. The 2-norm of the displacement vector for the second mode obtained for a cylinder of thickness $t = 0.05$, with a stiffener ring of thickness $t = 0.1$ (left) and without the stiffener (right).

ters, an augmentation of the potential-energy functional by introducing new unknowns, or computations over auxiliary meshes. Despite this simplicity, our method has been shown to be consistent with respect to the energy principle, so that the property of work equilibration, which has also been taken to be a key design principle in the derivation of constraint equations in [11], is fully satisfied.

Here we have assumed mesh conformity so that the intersection of the solid with the mid-surface of the shell can be represented in terms of the edges of the solid mesh. In this case, the assumption about mesh conformity is far less restrictive as compared with the alternative case of purely three-dimensional modelling, where generating a conforming solid mesh would not usually be practical and using special methods such as mortar finite elements would be a necessity in order to perform the coupling in very thin interfaces. We also note that a faithful implementation of our method depends on some global computations over the solid mesh to obtain the conjugate basis functions associated with the one-dimensional coupling interface. However, our current implementation avoids such computations by assuming the validity of certain local approximations. Although the simplified implementation has been show to give good results in our computational experiments, the validity of these approximations should be investigated in more detail with respect to the version requiring the global computation, but we leave this comparison to be a subject of a further study.

Funding

This work was supported by the Academy of Finland [Decision 346442].

References

[1] M. Benzi, G. H. Golub, and J. Liesen. Numerical solution of saddle point problems. *Acta Numerica*, 14:1–137, 2005. doi:https://doi.org/10.1017/S0962492904000212.

[2] H. J. Brauchli and J. T. Oden. Conjugate approximation functions in finite-element analysis. *Quarterly of Applied Mathematics*, 29(1):65–90, 1971. doi:https://doi.org/10.1090/qam/288470.

[3] D. Chapelle and K.J. Bathe. *The Finite Element Analysis of Shells - Fundamentals*. Springer, Berlin Heidelberg, second edition, 2011.

[4] R. D. Cook, D. S. Malkus, and M. E. Plesha. *Concepts and Applications of Finite Element Analysis*. Wiley, 1989.

[5] G. Guguin, O. Allix, P. Gosselet, and S. Guinard. Nonintrusive coupling of 3D and 2D laminated composite models based on finite element 3D recovery. *International Journal for Numerical Methods in Engineering*, 98(5):324–343, 2014. doi:https://doi.org/10.1002/nme.4630.

[6] M. Malinen. Finite elements and linear shell theory - Studies on shell models and numerical locking phenomena. Doctoral thesis, Helsinki University of Technology, 2001. Publications in Mechanics of Materials, TKK-LO-34.

[7] M. Malinen. Local reparametrization by approximating lines of curvature. *Mathematics and Computers in Simulation*, 201:275–290, 2022. doi:https://doi.org/10.1016/j.matcom.2022.05.016.

[8] L.E. Malvern. *Introduction to the Mechanics of a Continuous Medium*. Prentice-Hall, Englewood Cliffs, New Jersey, 1969.

[9] P.M. Naghdi. Foundations of elastic shell theory. In I.N. Sneddon and R. Hill, editors, *Progress in Solid Mechanics*, volume 4, pages 1–90. North-Holland, 1963.

[10] P. Råback, M. Malinen, J. Ruokolainen, A. Pursula, and T. Zwinger, editors. *Elmer Models Manual*. CSC - IT Center for Science, 1995-2022. URL: http://www.csc.fi/elmer.

[11] K. W. Shim, D. J. Monaghan, and C. G. Armstrong. Mixed dimensional coupling in finite element stress analysis. *Engineering with Computers*, 18:241–252, 2002. doi:https://doi.org/10.1007/s003660200021.

[12] K. S. Surana. Transition finite elements for three-dimensional stress analysis. *International Journal for Numerical Methods in Engineering*, 15(7):991–1020, 1980. doi:https://doi.org/10.1002/nme.1620150704.

[13] T. Yamamoto, T. Yamada, and K. Matsui. Numerical procedure to couple shell to solid elements by using Nitsche's method. *Computational Mechanics*, 63:69–98, 2019. doi:https://doi.org/10.1007/s00466-018-1585-6.

Mika Malinen, Peter Råback
CSC - IT Center for Science Ltd.
P.O. Box 405, FI-02101 Espoo, Finland
mika.malinen@csc.fi, peter.raback@csc.fi